Published in final edited form as:

Adv Funct Mater. 2024 August 08; 34(32): . doi:10.1002/adfm.202315040.

# Egg White Photocrosslinkable Hydrogels as Versatile Bioinks for Advanced Tissue Engineering Applications

Mahboobeh Mahmoodi<sup>1,2,3,4,5</sup>, Mohammad Ali Darabi<sup>1,2,3</sup>, Neda Mohaghegh<sup>1</sup>, Ahmet Erdem<sup>2,6</sup>, Amir Ahari<sup>1</sup>, Reza Abbasgholizadeh<sup>1</sup>, Maryam Tavafoghi<sup>2,3</sup>, Paria Mir Hashemian<sup>7</sup>, Vahid Hosseini<sup>1,2,3</sup>, Javed Iqbal<sup>2,8</sup>, Reihaneh Haghniaz<sup>1,2,3</sup>, Hossein Montazerian<sup>2,3</sup>, Jamileh Jahangiry<sup>2,3</sup>, Fatemeh Nasrolahi<sup>2,3</sup>, Arshia Mirjafari<sup>2,3</sup>, Erik Pagan<sup>8</sup>, Mohsen Akbari<sup>1,9</sup>, Hojae Bae<sup>10,11</sup>, Johnson V. John<sup>1</sup>, Hossein Heidari<sup>1</sup>, Ali Khademhosseini<sup>1,2,3</sup>, Alireza Hassani Najafabadi<sup>1,12</sup>

<sup>1</sup>Terasaki Institute for Biomedical Innovation, Los Angeles, California 90024, USA

<sup>2</sup>Center for Minimally Invasive Therapeutics (C-MIT), University of California, Los Angeles, California 90095, USA

<sup>3</sup>Department of Bioengineering, University of California, Los Angeles, California, USA

<sup>4</sup>Department of Biomedical Engineering, Yazd Branch, Islamic Azad University, Yazd 8915813135, Iran

<sup>5</sup>Joint Reconstruction Research Center, Tehran University of Medical Sciences, Tehran, Iran

<sup>6</sup>Department of Biomedical Engineering, Kocaeli University, Umuttepe Campus, 41001, Kocaeli, Turkev

<sup>7</sup>Department of Biomedical Engineering, Boston University, Boston, Massachusetts, USA

<sup>8</sup>Department of Botany, Bacha Khan University, Charsadda, Khyber Pakhtunkhwa, Pakistan

<sup>9</sup>Laboratory for Innovations in MicroEngineering (LiME), Department of Mechanical Engineering, University of Victoria, Victoria, British Columbia

<sup>10</sup>Department of Stem Cell and Regenerative Biotechnology, KU Convergence Science and Technology Institute, Konkuk University, Seoul 05029, Republic of Korea

<sup>11</sup>Institute for Materials Discovery, University College London, London, United Kingdom

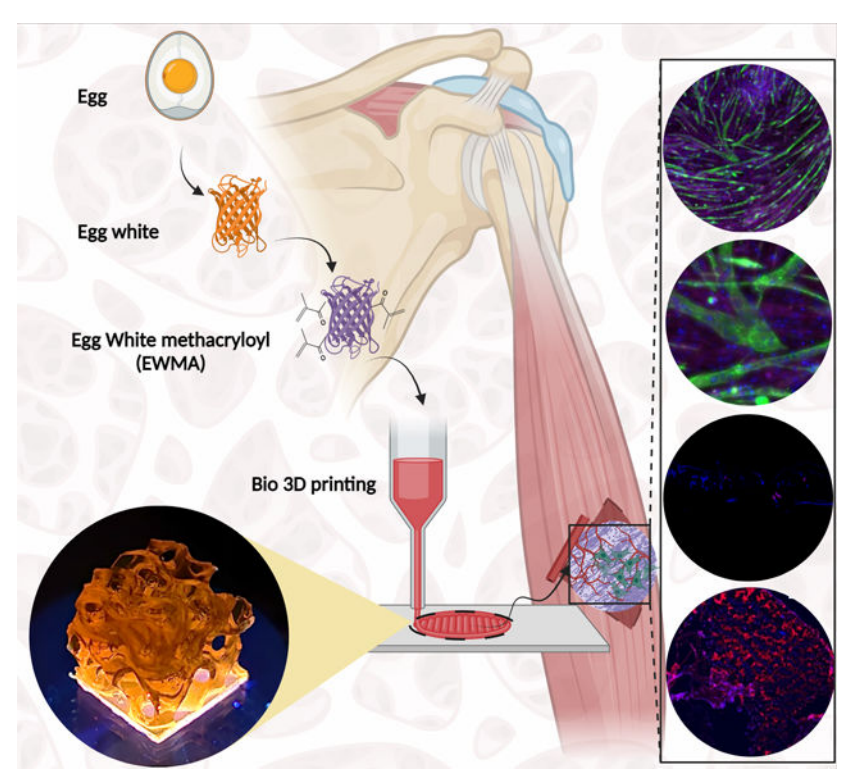
<sup>12</sup>Lundquist Institute for Biomedical Innovation, Harbor-UCLA Medical Center, Torrance, California, 90502, USA

#### Abstract

Three-dimensional (3D) bioprinting using photocrosslinkable hydrogels has gained considerable attention due to its versatility in various applications, including tissue engineering and drug delivery. Egg White (EW) is an organic biomaterial with excellent potential in tissue engineering. It provides abundant proteins, along with biocompatibility, bioactivity, adjustable mechanical properties, and intrinsic antiviral and antibacterial features. Here, we have developed a

photocrosslinkable hydrogel derived from EW through methacryloyl modification, resulting in Egg White methacryloyl (EWMA). Upon exposure to UV light, synthesized EWMA becomes crosslinked, creating hydrogels with remarkable bioactivity. These hydrogels offer adjustable mechanical and physical properties compatible with most current bioprinters. The EWMA hydrogels closely resemble the native extracellular matrix (ECM) due to cell-binding and matrix metalloproteinase-responsive motifs inherent in EW. In addition, EWMA promotes cell growth and proliferation in 3D cultures. It facilitates vascularization when investigated with human umbilical vein endothelial cells (HUVECs), making it an attractive replacement for engineering hemocompatible vascular grafts and biomedical implants. In summary, the EWMA matrix enables the biofabrication of various living constructs. This breakthrough enhances the development of physiologically relevant 3D *in vitro* models and opens many opportunities in regenerative medicine.

# **Graphical Abstract**



EW-derived hydrogel (EWMA) via methacryloyl modification enables 3D bioprinting. UV exposure triggers crosslinking, yielding bioactive hydrogels mimicking ECM. Compatible with diverse bioprinters, EWMA supports cell proliferation and endothelialization, promising applications in tissue engineering and regenerative medicine.

# Keywords

Egg white; Methacryloyl; Photocrosslinking; Endothelialization; Hydrogels; Bioink; 3D Bioprinting

# 1. Introduction

Engineering highly bioactive scaffolds that can accommodate cells and remodel *in vivo* is a fundamental goal in tissue engineering. Naturally derived hydrogels like gelatin, chitosan, and alginate have garnered significant interest due to their intrinsic biocompatibility and bioactivity. However, it's worth noting that they may not fully replicate the ECM or offer all the necessary nutrients for cells <sup>[1]</sup>. EW, a natural biomaterial, holds great potential in tissue engineering applications as it contains proteins such as ovalbumin (54%), ovotransferrin (12%), ovomucoid (11%), ovomucin (3.5%), and lysozyme (3.5%), which are essential for supporting cell survival and functionality. Furthermore, EW has exhibited remarkable antiviral, antibacterial, and anticancer properties, rendering it a suitable choice for applications in tissue engineering <sup>[2]</sup>. Compared to the commonly used natural proteins such as gelatin and collagen, EW provides a prevalent, accessible, and low-cost ECM that can be used directly in its raw form, thus eliminating the need for a complicated purification process <sup>[2a, 3]</sup>. Moreover, the non-mammalian source of EW reduces the risk of transmissible diseases, such as mad cow disease. It overcomes religious and cultural concerns associated with using mammalian-derived products <sup>[4]</sup>.

EW has been studied for various applications, including wound healing [5], tissue engineering [6], pharmaceuticals [7], and bioelectronics [2a]. EW-based hydrogels and cryogels exhibit functional properties such as stretchability, printability, and self-healing properties, as well as the capability to incorporate conductive nanomaterials for fabricating electronic sensors and actuators [8]. EW has been recently described as a substitute for ECMs to improve the angiogenesis and biocompatibility of bioscaffolds [6, 9]. EW has also been introduced as an alternative to Matrigel, a complex protein matrix with high angiogenic properties for mammary gland cells' 3D organotypic culture [9]. Despite high angiogenic properties, Matrigel lacks reproducibility as it is secreted by living cells [10]. Moreover, the tumor cell source of Matrigel may limit its use in the human body [11]. Like Matrigel, EW can induce the formation of prevascular networks in endothelial and smooth muscle cell co-cultures [7]. The EW matrix supports the growth of various cell types from human, mouse, and rat origins, and it has demonstrated compatibility with the aortic ring assay, enabling the culture of vascular and tumor cells [12]. HUVECs and rat aortic endothelial cells appeared to grow, migrate, and organize themselves in a vessel-like network within 48 hr in an EW matrix similar to that observed for the Matrigel [10a]. However, little is known about the potential of EW hydrogels for the endothelization of biomaterial surfaces [13].

Endothelization of biomedical implants has been widely accepted as an ideal approach to improve biocompatibility and avoid implant rejection  $^{[14]}$ . Furthermore, a highly integrated endothelial lining is needed on the lumen surface of artificial vascular grafts to improve their hemocompatibility and long-term patency  $^{[15]}$ ; however, it is significantly challenging to form a confluent endothelium layer on biomaterial surfaces  $^{[15]}$ . Based on previous studies that demonstrated the high activity of endothelial cells in  $EW^{[12]}$ , one can hypothesize that EW can be used as a highly bioactive substrate to induce endothelialization. Also, the high cell affinity of albumin, a significant protein in EW, can improve bioactivity and reduce the complexity of introducing cell-binding domains in  $EW^{[2a, 16]}$ .

Here, we develop EW hydrogels that can be readily crosslinked through light irradiation, forming a highly bioactive ECM-mimetic microenvironment for biological compounds. In contrast to thermal or chemical crosslinking techniques, photocrosslinking will create hydrogels with tunable mechanical and physical properties that are easily microfabricated using various light-based methods, such as photomasking and stereolithography, to generate miniaturized structures. Also, photocrosslinking of EW eliminates the need for high temperatures conventionally involved in thermal crosslinking processes, thus providing opportunities for 3D culture and cell encapsulation within the hydrogels [17]. To prepare a photocrosslinkable hydrogel bioink, we modified EW with methacrylic groups to form an EWMA hydrogel that can be crosslinked with light in the presence of photo-initiators (PIs). We performed physical and mechanical characterizations, including biodegradation, compression, and rheological analysis, to evaluate the strength and stability of the synthesized EWMA hydrogel under physiological conditions. Furthermore, we assessed the potential of EWMA hydrogels as a cell-laden ECM that can be used for bioprinting and tissue engineering applications. For this purpose, we evaluated cell functions, cytocompatibility and metabolic activity of different cell types encapsulated within EWMA hydrogels. Also, we investigated the efficacy of EWMA hydrogels as an ECM to host endothelial cells and induce endothelization in a 2D culture of HUVECs.

# 2. Results and Discussions

#### 2.1. Chemical characterizations and crosslinking kinetics

EWMA was synthesized in DPBS buffer using a one-pot method that yielded a white-yellowish foam (Figure 1A, S1). During the methacryloyl modification of EW, the acidic by-product of the reaction (methacrylic acid) can drastically decrease the solution pH and inhibit the substitution reaction by protonating the free amino groups of lysine on EW  $^{[18]}$ . Therefore, the pH of the solution was monitored and maintained in a basic range between 8 and 9 to favor the forward reaction by deactivating the acidic by-products. The methacryloyl modification of EW was verified by HNMR analysis (Figure 1B, S2). The peak area for amino acid moieties at 7.2 ppm was used to normalize the HNMR spectra since this area remained unchanged after methacryloyl substitution. HNMR spectra showed that the peak intensity for the methylene proton (NH<sub>2</sub>CH<sub>2</sub>CH<sub>2</sub>CH<sub>2</sub>CH<sub>2</sub>-) of free lysine at 2.9 ppm decreased drastically on EW after the reaction. On the other hand, the acrylic protons (CH<sub>2</sub>=C(CH<sub>3</sub>)CONH-) at 5.7–5.3 ppm and methyl protons (CH<sub>2</sub>=C(CH<sub>3</sub>)CO-) at 1.8 ppm were increased for EWMA, confirming the methacryloyl modification of EW. The degree of substitution (DS) of EWMA was calculated to be 74.6% by comparing the methylene proton intensity around  $\delta$ =2.9 ppm for the methacrylated and pristine EW.

The EWMA hydrogels were synthesized by mixing EWMA and PIs, followed by photocrosslinking with UV irradiation. A rheological test was carried out to investigate the gelation kinetics of EWMA under UV light. Figure 1C–E represents the crosslinking kinetics of the hydrogels. Upon irradiation with UV light, the crosslinking reaction started until the gelation point was reached (where G' surpassed G'') within ~4–20 s. This point corresponds to a sharp increase in the storage modulus when enough free radicals are generated to drive the reaction. Overall, a shorter gelation time was observed for hydrogels

containing higher percentages of vinyl groups, accelerating the polymerization process (Figure 1D and E). EWMA 5% exhibited a significantly longer gelation time than GelMA 5%, which can be explained by fewer vinyl groups on EWMA 5%. Additionally, the higher amount of vinyl groups on EWMA 10% resulted in a significantly shorter gelation time than EWMA 5%. With the increase in crosslinking time, the reaction rate became slower until the storage modulus reached a plateau at UV irradiation time ~1 min, which was used as a crosslinking time to prepare hydrogels for the rest of the characterizations.

#### 2.2. Mechanical and physical characterization of EWMA hydrogels

Scanning electron microscopy (SEM) characterizations (Figure 2A) showed that the hydrogels had a porous structure, which is critical for cell growth and metabolism [19]. As shown in Figure 2B, the porosities of GelMA 5% ( $96\pm0.9\%$ ), EWMA 5% ( $99\pm0.87\%$ ), and EWMA 7.5% (96±1%) were comparable while EWMA 10% (88±1%) showed a significantly lower degree of porosity compared to these samples. Mechanical robustness is one of the critical factors to consider for the design of bio-scaffolds to support the dynamic motion of tissues, especially at load-bearing sites [20]. The mechanical characteristic of hydrogels was evaluated using compression testing, as shown in Figure 2C and D. The compressive modulus for the EWMA hydrogels (Figure 2C) increased with the increase of EWMA concentration due to the increase in crosslinking density on the samples. The compressive modulus for EWMA 5% (112±9.9 kPa) and 7.5% (136± 5.9 kPa) was comparable to that of the control, GelMA 5% (133±7.3 kPa); however, EWMA 10% (166±13.7 kPa) showed the highest compressive modulus. Similarly, the failure strength (Figure 2D) of the EWMA hydrogels raised with the increase in EWMA concentration. Also, the failure strength for EWMA 7.5% (99±6.5 kPa) and 10% (178±5 kPa) was higher than that for GelMA 5%; however, EWMA 5% (29±2.9 kPa) showed a significantly lower strength.

While compressive strength is vital for designing mechanically sturdy scaffolds, it's equally important to consider factors such as porosity and stiffness. These elements can significantly impact nutrient transport to the enclosed cells and influence bioactivity <sup>[21]</sup>. As discussed previously, EWMA 7.5% showed comparable stiffness and porosity to the GelMA 5%, while its mechanical strength was significantly higher. Therefore, among different concentrations of the EWMA hydrogel, EWMA 7.5% was chosen for further efficacy study of the hydrogels, as will be discussed in the experimental section.

The swelling of hydrogels post-implantation can lead to tissue compression and negatively affect their mechanical characteristics <sup>[22]</sup>. Hydrogels with lower swelling ratios have shown higher mechanical robustness and a more stable ECM microenvironment to maintain the microstructural remodeling of tissues after implantation <sup>[23]</sup>. The swelling ratio of the hydrogels is shown in Figure 2E. Overall, the EWMA hydrogels at all concentrations showed lower swelling ratios than GelMA hydrogels. The swelling ratios of the hydrogels incubated for 10 hr were 5.7, 3.9, and 4.4 for EWMA 5%, 7.5%, and 10%, respectively, which were significantly less than the swelling ratio of GelMA 5% (7.9). These findings suggest that EWMA offers a physically stable hydrogel, providing a dependable platform for studying cellular behaviors. It maintains its structural integrity without significant changes

during the incubation and culture period <sup>[22c, 24]</sup>. Besides, hydrogels should experience controlled degradation following implantation to facilitate tissue regeneration and *in vivo* remodeling. Nonetheless, a rapid degradation rate prior to complete tissue regeneration can lead to suboptimal mechanical performance <sup>[23]</sup>. As shown in Figure 2F, GelMA 5% completely degraded in a collagenase type II solution only in 2 days, while the weight loss for EWMA hydrogels was less than 20% even after incubation for 10 days. Therefore, EWMA hydrogels with a moderately lower degradation rate than GelMA can provide a more robust hydrogel matrix for tissue regeneration *in vivo* <sup>[25]</sup>.

# 2.3. Rheological characterization of EWMA hydrogels

In Figure 3, the storage and loss moduli are presented against oscillatory shear strain and angular frequency for crosslinked EWMA and GelMA hydrogels. It's worth noting that the storage modulus (G') consistently surpassed the loss modulus (G") across all samples, as depicted in Figures 3A and 3B, owing to their crosslinked nature [26]. The storage and loss moduli offer valuable insights into the mechanical behavior and properties of viscoelastic materials. Typically measured as a function of angular frequency, these moduli's behavior at different frequencies provides crucial information about the material's response under varying deformation rates. Figures 3C and D display the relationship between storage and loss moduli and angular frequency. GelMA 5% and EWMA 5% showed comparable storage modulus (at angular frequency=1 rad s<sup>-1</sup> and strain=0.1%) as well as loss modulus; however, the moduli increased with the increase in EWMA concentration due to the increase in methacrylate contents and crosslinking density on the hydrogels (Figure 3E and F). To illustrate, the storage modulus of EWMA 10% reached a substantial 6570 Pa, which was notably 14 times higher than that of EWMA 5% at 466 Pa. Similarly, the loss modulus of EWMA 10% measured 1480 Pa, exceeding that of GelMA 5% at 64 Pa by a factor of 23.

#### 2.4. Biological activity of EWMA hydrogels

2.4.1 3D printing of constructs using EWMA as a bioink—Figure 4A–I represent the 3D printing endeavor using the Digital Light Processing (DLP) stereolithographic (SLA) technique for EWMA constructs. These images provide a comprehensive view of the printed Y-shaped perusable hydrogel construct from various isometric and top angles (Figure 4A, 4B, and 4C), with a detailed close-up of the bifurcation (d). Additionally, Figure 4E presents a close-up view that highlights the printed layers and the staircase effect observed in the channel walls. The successful perfusion of red and blue dye through the bifurcation illustrates the construct's perfusability and possibility of printing various structures using EWMA as a bioinks (Figure 4F). The 3D design of the Y-shaped bifurcation is displayed in Figure 4G, while Figure 4H demonstrates a gyroid print with eight-unit cells across and a 500 µm wall thickness. Lastly, Figure 4I-J offers a visual representation of the gyroid's thin members. This collectively highlights the precision and complexity achievable through light-based additive manufacturing in creating intricate and functional constructs using the SLA-optimized EWMA bioink formulation. The results suggest that EWMA holds promise for use in various printing applications and precision bio-printing methodologies, showcasing its versatility and potential.

Furthermore, we investigated the printability of EWMA using an extruder-based 3D printer (BioX cell). Our findings clearly demonstrated the ease with which EWMA can be printed using this extruder printer. Moreover, our results indicated that, with EWMA, it is feasible to achieve multicolor printing, enabling the representation of two or even more distinct cell types printing within a single construct, as illustrated in Figure S3. The process of printing EWMA utilizing the BIOX cell is visually detailed in the supplementary video. In conclusion, the findings underscore the potential of EWMA in a wide array of printing applications and bio-printing techniques, highlighting its versatility and promise.

**2.4.2 Vascularization and endothelial cell activity**—Matrigel has been widely used as a matrix for angiogenesis assays due to its ability to form 3D vascular networks. However, the angiogenic activity of Matrigel strongly depends on the composition of its growth factors, resulting in low-reproducibility assays due to variation in Matrigel composition <sup>[27]</sup>. Similar to Matrigel, the EW hydrogels have shown the ability to form vessel-like endothelial networks <sup>[10a]</sup>. Therefore, the methacryloyl modification of EW can provide a photocrosslinkable and naturally derived hydrogel with the ability to form a highly biocompatible and endothelial cell-friendly ECM for angiogenesis in tissue engineering and drug testing.

Figure 5 shows the cytocompatibility of hydrogels seeded with endothelial cells (2D culture). Fluorescence images reveal successful adhesion and growth of HUVECs on the surface of the EW hydrogels (Figure 5A). EWMA 7.5% was thoroughly covered with a layer of HUVECs on day 7 of culture. Besides, the *PrestoBlue*<sup>™</sup> assay (Figure 5B) showed that the metabolic activity of HUVECs on day 7 of culture was significantly higher for EWMA hydrogels than for the GelMA hydrogel. The activity of endothelial cells on the surface of EWMA 7.5% was further confirmed by VE-cadherin/DAPI immunostaining of Green fluorescent protein- human umbilical vein endothelial cells (GFP-HUVECs) (Figure 5C). VE-cadherin is an endothelial-specific adhesion molecule located at junctions between the endothelial cells. VE-cadherin plays a critical role in blood vessel formation and angiogenesis by regulating various cellular processes, such as cell proliferation and apoptosis, and modulating vascular endothelial growth factor (VEGF) functions [28]. The expression of VE–cadherin (red) on EWMA7.5% confirmed the formation of adherents' junctions between endothelial cells on the surface of this sample.

We evaluated the vascularization of EWMA 7.5%, GelMA 5% and Matrigel using GFP-HUVECs seeded on the surface of the hydrogels (Figure 6). For the vascularization assay, the samples were placed in the incubator while shaken on a plate shaker to trigger cell division and growth <sup>[29]</sup>. As discussed in the section 2.2, among different concentrations of EWMA hydrogels, EWMA 7.5% was chosen for the vascularization assay due to its porosity and stiffness being comparable to those of the control sample, GelMA 5%. As shown in Figure 6, the cell spreading on day 4 of culture was 93% on EWMA 7.5%, while it was 60% and 22% on GelMA 5% and Matrigel, respectively. These results indicated higher endothelial cell activity on the EWMA hydrogel surface compared to other naturally derived hydrogels, such as GelMA and Matrigel, which can be attributed to the presence of cell-binding motifs and integrin receptors in EW. For example, the presence of cystatin in EW acts as a TGF-β receptor and regulates integrins, which are the main receptors for ECM

[9]. Rapid vascularization of EWMA hydrogels can improve its biocompatibility and reduce the failure rate of vascular implants, demonstrating the high potential of EWMA as ECMs in vascular tissue engineering and angiogenesis testing.

However, unlike Matrigel tested under the same conditions, the EWMA hydrogel did not facilitate the formation of vascular networks (Figure 6). Matrigel is an extract of proteins and biomolecules derived from mouse tumors, and its vascularization property is attributed to a carcinogenic nature and components rich in VEGF and ECM proteins, such as laminin, closely mimicking the complex environment of the basement membrane [11, 30]. In an earlier study by Mousseau et al., it was shown that similar to Matrigel, the "thermally" crosslinked EW can also support the formation of vascular networks [10a]. The vascularization of EW has been attributed to its micropatterns and functional proteins, such as cystatin and avidin. These proteins contain major integrin receptors and Arg-Gly-Asp (RGD)-mimicking amino acid domains that can play a critical role in cell adhesion and organization [9-10]. However, the methacrylation of EW resulted in vinyl groups occupying the cell binding sites on EW, thus altering the endothelial cell spreading pattern and vascularization of EWMA hydrogel. Furthermore, the photocrosslinking process may have led to variations in the stiffness of the EW gel compared to thermally crosslinked EW, potentially altering the local fiber structures and microenvironments essential for cell growth and the development of vascular networks. The critical role of matrix stiffness on the growth of endothelial cells and vascularization is also reported by other researchers [31]. Zhao et al. reported that the substrate stiffness can increase the migration and angiogenesis potential of HUVECs [32]. Substrate stiffness can also influence the morphology, cytoskeletal structure, and adhesion of endothelial cells. Cells generate large forces on the stiff substrates using actin-myosin complexes, which are part of the cytoskeleton, to form the mature focal adhesion. In contrast, the soft substrates cannot provide sufficient resistance to counterbalance large, cell-generated forces. Thus, cells cannot provide abundant stress fibers, adhere to them, and grow well on soft surfaces. Also, stiff substrates can support cell spreading, whereas soft substrates induce rounded cell morphologies. Enhancing tissue regeneration can be achieved by optimizing scaffold stiffness at the surface. Therefore, the stiffness of scaffolds is an important factor in tissue engineering, which can affect the differentiation, proliferation, and migration of cells on the surface of scaffolds and regulate angiogenesis and vascularization processes [33].

In conclusion, EWMA hydrogels have emerged as promising tools for promoting endothelialization and vascularization due to their rich composition of bioactive molecules, including growth factors, peptides, and proteins. The diverse components within EWMA, such as fibronectin and collagen, play vital roles in enhancing endothelial cell adhesion, migration, and proliferation. Moreover, the mechanical properties of EWMA hydrogels, such as stiffness and viscoelasticity, significantly influence endothelial cell behavior by facilitating cell adhesion, migration, and alignment through mechanotransduction pathways. Additionally, the biodegradability of EWMA hydrogels allows for controlled degradation, creating space for endothelial cell infiltration, proliferation, and the formation of new blood vessels. Furthermore, EWMA hydrogels can be engineered to encapsulate bioactive molecules for sustained release, providing continuous signaling cues that promote endothelial cell proliferation, migration, and angiogenesis within the hydrogel construct [34].

# 2.5. Cytocompatibility of 3D bioprinted EWMA constructs encapsulating myoblast cell line

The cytocompatibility of the hydrogels was evaluated using C2C12 cells in 3D culture (Figure 7). The C2C12 cells were encapsulated in the EWMA (5%, 7.5%, and 10% w/v) and GelMA (5% w/v) bioinks and injected to print lines by using 18 gauge metal blunt tipped dispensing needles. The cell differentiation was assessed by immunofluorescent staining (Figure 7). As is evident from the images (Figure 7A), the C2C12 cells were successfully encapsulated within the hydrogels. Also, DAPI/Phalloidin fluorescence images showed a homogenous distribution of cells in all samples (Figure 7A). However, the cells encapsulated in GelMA and EWMA showed different levels of differentiation after 7 days of culture. The myotube coverage area was comparable between GelMA 5% and EWMA 5% at 12.3% ± 1.9 and 11.5%  $\pm$  1.4, respectively. However, the cells encapsulated in EWMA 7.5% showed a significant increase in their myotube coverage area at  $32.3\% \pm 3.2$ . In contrast, increasing EWMA concentration to 10% did not favor cell differentiation and showed the lowest myotube coverage area at only  $4.8\% \pm 1.3$  (Figure 7B). The nuclei distribution per myotube quantification data also confirmed that C2C12 cells fused more efficiently and formed larger myotubes in EWMA 7.5% compared to other hydrogels (Figure 7C). While both GelMA 5% and EWMA 5% showed comparable levels of cell fusion, increasing EWMA concentration to 10% drastically limited the ability of the cells to fuse. This decreased cell fusion and differentiation can be attributed to the increase in stiffness and less nutrition transfer at higher polymer concentrations [35]. Our results showed that EWMA 7.5% and GelMA 5% had comparable stiffnesses and porosities (Figure 2) suitable for nutrient transfer and cell proliferation; therefore, the higher cell activity observed on EWMA 7.5% in comparison to GelMA 5% can be attributed to the EWMA 7.5% hydrogel being intrinsically more bioactive than the GelMA 5% hydrogel.

#### 2.6. Assessing in vivo biocompatibility of EWMA

To assess the biocompatibility of EWMA hydrogels post-implantation, *in vivo* investigations were conducted involving the subcutaneous implantation of both GelMA 5% and EWMA 7.5% hydrogel scaffolds. Detailed morphological examination of the skin through H&E staining (Figure 8A and B) revealed the absence of inflammation or toxicity associated with GelMA 5% or EWMA 7.5% hydrogels. Remarkably, after 30 days, enhanced vascularization was observed in the EWMA group compared to GelMA, evident by the presence of blood vessels (indicated by red color) immune fluorescent staining (Figure S5). In addition, GelMA 5% samples showed evidence of slight fibrosis, characterized by H&E, which can be attributed to the degradation and side product of GelMA (Figure 8C).

For the subcutaneous implantation samples, immunohistochemical staining was conducted. F4/80 is a well-established marker used to identify mouse macrophage populations [36], particularly CD80 associated with pro-inflammatory subtypes [37]. Detection of the CD80 marker can reveal inflammation in the implanted region. Figure 8C displays immunohistochemical staining of the full-thickness skin near the subcutaneous implantation site. We utilized F4/80 (red) and CD80 (Green) [38] markers in conjunction with a nuclear stain (blue). Consistent with our finding in H&E staining, minimal CD80 pro-inflammatory marker staining was observed in all samples, indicating the absence of

inflammation associated with EWMA 7.5% and GelMA 5% implantation. In summary, the immunohistochemical analysis indicated no sign of inflammation or activation of the immune system, which indicated that EWMA can serve as promising photocrosslinkable hydrogel. Furthermore, evaluation of vital organs, including the heart, kidney, liver, and lungs, alongside skin tissues, demonstrated no significant indications of adverse immune responses or toxicity. These findings, as illustrated in Figure 8D, emphasize the promising biocompatibility of EWMA hydrogels, positioning them as potential candidates for diverse biomedical applications, particularly in tissue engineering and regenerative medicine.

# 3. Conclusion

Here, we synthesized naturally derived photocrosslinkable hydrogels based on an EWMA that can be used as a bioactive ECM for a variety of tissue engineering applications. EWMA can be crosslinked with UV light in the presence of PIs, resulting in the formation of EWMA hydrogels with tunable mechanical and physical properties. The EWMA hydrogels showed a high cytocompatibility with different mammalian cell lineages, such as fibroblasts and endothelial cells. In addition, EWMA hydrogels highly supported the growth and proliferation of endothelial cells, resulting in the formation of a dense layer of functional endothelial cells expressing an endothelial-specific adhesion molecule, VE-cadherin, on the surface of EWMA hydrogels. The endothelization of EWMA was significantly higher than GelMA, which is a photocrosslinkable hydrogel widely used for tissue engineering applications. The endothelial cell proliferation on EWMA was also significantly higher than on Matrigel, a complex protein matrix with superior angiogenic and vascularization properties. Overall, our findings demonstrated a high potential of EWMA as a prevalent, inexpensive, and non-mammalian source of functional proteins, such as ovalbumin, for the creation of highly bioactive ECMs and endothelization of vascular grafts in tissue engineering. Indeed, more research needs to be done to find out the protein content and chemistry of eggs from different sources and show how batch differences affect the physical and chemical qualities of EWMA.

# 4. Experimental Section/Methods

#### **Materials**

The EW used in this work was extracted from commercially available eggs. The methacrylic anhydride (MA, purity 94%), dimethyl sulfoxide (DMSO, purity 99%), Triton X-100, and 2-hydroxy-4'-(2-hydroxyethyl)-2-methyl propiophenone (purity 98%) were obtained from Sigma Aldrich. Growth factor reduced Matrigel was purchased from BD Biosciences, San Jose, CA, USA. Collagenase type II was obtained from Thermo Fisher Scientific. Dulbecco's phosphate-buffered saline (DPBS), trypsin-ethylenediaminetetraacetic acid (EDTA), Dulbecco's Modified Eagle Medium (DMEM), and penicillin/streptomycin (Pen/Strep) were purchased from Gibco, NY, USA. Fetal bovine serum (FBS) and bovine serum albumin (BSA) were supplied from Sigma-Aldrich. Endothelial cell culture system (EGM™-2 Endothelial Cell Growth Medium-2 BulletKit™) containing endothelial basal medium (EBM) and endothelial growth factors (EGFs) were obtained from Lonza, Basel, Switzerland. Vascular endothelial-cadherin (VE-cadherin, 7B4 or cadherin-5, GT 15250)

antibody and AlphaBioCoat Solution (AC001) were obtained from Neuromics (a division of CA3 Biosciences, Inc). A highly cross-adsorbed Donkey anti-Goat IgG (H+L) secondary antibody was purchased from Biotium. *PrestoBlue*, Live/Dead cell viability/cytotoxicity kit, PE conjugated anti mouse CD80, FITC conjugated anti mouse F4/80, and DAPI/Phalloidin staining were manufactured by Invitrogen and purchased from Fisher Scientific, USA. Paraformaldehyde in 0.1 M phosphate buffer was obtained from Bioenno Tech, USA. All reagents were used without further purification.

#### **EWMA** synthesis

EW was collected from fresh eggs and filtered two times through a mesh net (50–100 μm) to remove impurities (the EW was collected from a large batch of eggs to ensure the reproducibility and consistency of the product, n=4 experiments and each time we used at least 100 eggs, Table S1). To prepare a homogenized and clear EW solution, EW was diluted with equal water weight and vigorously stirred for 1 hr at 4 °C. The solution was subsequently centrifuged at 5000 rpm for 20 min, and the supernatant was collected and freeze-dried (Free zone freeze dryer, Labconco, MO, USA) before the methacryloyl modification [13]. EWMA was synthesized in DPBS using a one-pot synthesis method. Firstly, 4.5 g of EW was dissolved in 112.5 ml of DPBS (pH= 7.4) and mixed for 1 hr at 4 °C to obtain 4% w/v EW solution [18, 39]. The solution was then centrifuged at 3500 rpm for 5 min, and the supernatant was used to synthesize EWMA. To prepare medium EWMA (M-EWMA substitution degree of ~74.6%), 1.8 ml of MA was added to the reaction mixture dropwise, followed by continuous stirring overnight in an ice-covered container. The pH of the reaction solution was regularly monitored and kept between 8 and 9. The monitoring of pH was crucial for the methacryloyl modification reaction since the acidic by-product of the reaction (methacrylic acid) could decrease the pH of the solution, thus inhibiting the forward reaction by protonating free amino groups of EW [18]. After the overnight reaction, the reaction mixture was centrifuged at 5000 rpm for 15 minutes to remove air bubbles. The solution was then dialyzed against deionized (DI) water using a dialysis membrane of 12-14 kDa at 4 °C to remove the unreacted MA and the by-products. Finally, the EWMA solution was lyophilized in the freeze-dryer and stored at 4°C for future use. Different types of EWMA molecules such as low substituted EWMA (L-EWMA) and high substituted EWMA (H-EWMA) were also synthesized by adding 0.9 and 3.6 ml of MA, respectively. However, we selected the M-EWMA since the L-EWMA (DS of 47.2 %) did not provide adequate crosslinking densities, and the H-EWMA (DS of 85.4 %) performed the same as the M-EWMA (Figure S2). In all experiments, GelMA (DS 63.8%, prepared as previously described [17, 40]) with a concentration of 5% w/v was used as the control sample. EWMA with the concentrations of 5% w/v, 7.5% w/v, and 10% w/v were named EWMA 5% EWMA 7.5%, and EWMA 10%, respectively.

#### Chemical characterization of EWMA

<sup>1</sup>H NMR spectroscopy was used to determine the degree of methacrylation of EWMA following the same method used for methacrylated gelatin (GelMA) <sup>[41]</sup>. To prepare the samples for NMR analysis, EW and EWMA were dissolved in DMSO at room temperature at a concentration of 2% w/v. The primary amino groups of EW proteins, originating from the amino acid lysine, interact with methacryloyl groups. As a result, these amino groups are

critical for calculating the substitution degree of EWMA. The peak area for primary amino groups around  $\delta$ = 2.9 was measured for EW before and after methacloyl modication. The DS was calculated based on Equation 1 <sup>[42]</sup>

$$DS = \left(1 - \frac{Lysine methylene proton of EWMA}{Lysine methylene proton of pristine EW}\right) \times 100\%$$
(1)

#### **EWMA** hydrogel preparation

EWMA pregel solutions at concentrations of 5, 7.5, and 10% w/v were prepared by dissolving 50, 75, and 100 mg of EWMA in DI water, respectively. Also, a widely used naturally derived biopolymer, GelMA, was prepared as a control at a concentration of 5% w/v. Subsequently, an ultraviolet (UV) PI, 2-hydroxy-4'-(2-hydroxyethyl)-2-methyl propiophenone (5 mg ml<sup>-1</sup>), was added to the pregel solutions. The hydrogels were formed by photocrosslinking the pregel solutions with 356 nm UV light at an intensity of 800 mW for 1 min (distance from the light source: 8 cm).

#### Crosslinking kinetics of EWMA hydrogels

The crosslinking kinetics of the hydrogels were evaluated by real-time monitoring of variations in the storage (G') and loss modulus (G'') under UV light using an MCR 302 rheometer (Anton Paar, Graz, Austria). Rheological measurements in the oscillatory mode were performed on 100  $\mu$ l of the prepolymers using a sandblasted measuring plate (PP08/S, diameter= 8 mm). Oscillatory displacements with 1% strain and 1 Hz frequency were applied to the hydrogels, and UV irradiation was commenced after a 1 min stabilization period. The modulus versus UV irradiation time ( $\sim$  4 min) was recorded until an entire plateau was achieved. The gelation point was assigned to the time when the storage modulus surpassed the loss modulus for each measurement.

#### Morphological characterizations

SEM analysis was carried out to analyze the physical structure and porosity of the hydrogels. The porosity of the hydrogels was determined by analyzing SEM images with ImageJ software. The crosslinked hydrogels were lyophilized in a freeze-dryer. The lyophilized samples were then coated with iridium using an ion beam sputter deposition and etching system (IBS/e, South Bay Technology, CA, USA). SEM images were captured on a Supra 40 VP, Zeiss microscope, Germany, at an accelerating voltage of 2 kV.

# Swelling test

To evaluate the swelling ratio of EWMA hydrogels, disc-shaped hydrogel samples (diameter=8 mm, height=2 mm) were crosslinked, and samples were weighed ( $W_0$ ). The discs were then immersed in DPBS and incubated at 37 °C. The hydrogel discs were removed from DPBS at different time points (0, 1, 2, 4, 6, 8, 10, 24, and 48 hr), the excess DPBS was removed using Kimwipes, and the samples were weighed again ( $W_t$ ). The increase in the volume of the samples was directly related to the amount of DPBS absorbed,

and the swelling ratio was calculated based on Equation 2 <sup>[43]</sup>. Each condition was tested with four replicates, and the results were subsequently averaged.

Swelling ratio = 
$$\frac{W_{\tau} - W_0}{W_0} \%$$
 (2)

# **Degradation test**

To evaluate the *in vitro* degradation of EWMA hydrogels, disc-shaped samples were prepared following the method explained in the previous section. The samples were then immersed in DPBS containing collagenase type II (2.5 U/ml) and incubated at 37 °C. At desired incubation times (1, 2, and 10 days), the samples were removed from DPBS, freeze-dried, and weighted. The weight loss percentages of the samples were calculated based on Equation 3, where  $W_i$  and  $W_f$  are the initial and final weights of samples after immersion in DPBS, respectively. We conducted four replicates for each condition and then calculated the average results.

Weight loss 
$$\left(\%\right) = \frac{W_i - W_f}{W_i} \times 100$$
 (3)

# **Compression test**

To prepare samples for compression testing, we transferred 80  $\mu$ l of EWMA pregel solutions into cylindrical poly(dimethylsiloxane) (PDMS) molds (height= 2 mm, diameter= 8 mm) and crosslinked them. Subsequently, the hydrogels were soaked in DPBS for 1 hour at room temperature prior to measurements. We evaluated the compression properties of the samples using an Instron 5542 machine (Norwood, MA, USA) with a strain rate of 1 mm/min. The compressive modulus was determined from the slope of the linear region of stress-strain curves, up to a strain of 0.1 mm/mm. The compressive strength was defined as the maximum stress at the point of failure. We conducted four replicates for each condition and then calculated the average results.

#### Rheological characterizations

To assess the rheological behavior of the hydrogels, we prepared disc-shaped samples using the same crosslinking method employed for compression testing. Afterward, these samples were allowed to equilibrate in DPBS for 1 hour at room temperature. We examined the rheological properties of the hydrogels using an MCR 302 rheometer equipped with a sandblasted measuring plate (PP08/S) having a diameter of 8 mm. Oscillatory shear strain tests, ranging from 0.01% to 100%, and frequency sweeps covering an angular frequency range of 0.1 to 100 rad/s at a fixed strain of 0.1%, were conducted on the hydrogels at approximately 25 °C. Storage modulus (G') and loss modulus (G'') were determined as functions of shear strain and angular frequency, with G' and G'' values reported at an

angular frequency of 1 rad/s and a strain of 0.1%. We conducted five replicates for each condition and subsequently reported the average values.

# 3D bioprinting using EWMA

A digital micro-mirror (DMD) based light modulator was used in conjunction with a 385nm LED to produce an image with an effective pixel size of 27 µm at the focal plane. The print layer height for this SLA setup was 50 µm with an exposure time of 10s/layer and an intensity of 28 mW cm<sup>-2</sup> with a 95%< uniformity cross the print plane. The dark time between layers was set to 0.5 s to eliminate dark polymerization induced pattern warping. The designed Y-shaped bifurcation had a wall thickness of 200 µm (~7 pixels across) and an internal diameter of 1.5 mm and was printed horizontally with layers parallel to the channel direction. This was especially challenging considering the low stiffness and high compliance of EWMA hydrogel. The PI Lithium phenyl (2,4,6-trimethylbenzoyl) (LAP) was used at a concentration of 1% w/v, and the photo-absorber tartrazine was used at a concentration of 0.3% w/v to achieve the optimal exposure profiles for the given optical configuration.

Furthermore, we conducted EWMA printing using the extruder perimeter of the Bio X printer. Briefly, we initially dissolved freeze-dried EWMA in DI water, achieving a concentration of 7.5%. Subsequently, we mixed this EWMA solution with water-based coloring agents, either green or pink, creating distinct colors for visualization. The prepared mixture was then loaded into a 3 ml syringe, which was subsequently affixed to the printer. The printing procedure was executed in accordance with the manufacturer's recommended settings, involving specific conditions such as a temperature of 17 °C, a pressure range of 90–100 Pa, a printing speed of 9 mm S<sup>-2</sup>, and an adjusted bed temperature of 7 °C. These controlled parameters ensured the successful and precise printing of EWMA-based structures, offering versatility in color representation and material properties for potential applications in tissue engineering and beyond.

#### The cytocompatibility of EWMA hydrogels

Endothelialization and cytocompatibility study of EWMA hydrogels using a 2D endothelial cell culture.

Endothelial cell culture and seeding on the hydrogels: Green fluorescent protein-human umbilical vein endothelial cells (GFP-HUVECs, Neuromics) were cultured in EBM supplemented with BulletKit EGFs and 1% v/v Pen/Strep in a 5% CO<sub>2</sub> incubator at 37 °C. GFP-HUVECs were cultured in a T25 Corning cell culture flask pre-treated with AlphaBioCoat solution. At the confluence of ~80%, cells were enzymatically detached from the flask using 0.25% trypsin-EDTA and collected by centrifugation at 1200 rpm for 5 min. Cells were resuspended in the media and counted using a hemocytometer (JuLI<sup>TM</sup> Br Live Cell Analyzer). Then, 100  $\mu$ l of media containing 7.5 × 10<sup>5</sup> of GFP-HUVECs was transferred to the surface of samples.

**Endothelial cell activity and immunostaining:** GFP-HUVECs seeded on the surface of the hydrogels were imaged over 7 days using a fluorescence microscope. PrestoBlue assay was performed following the method described previously to measure the metabolic activity of GFP-HUVEC cells seeded on the surface of the hydrogels on days 1, 3, and 7 of culture.

VE-cadherin/DAPI immunostaining was performed to observe the endothelial cell-to-cell junctions on the surface of the EWMA 7.5% hydrogel following protocol [44]. Briefly, the hydrogels were removed from the incubator on day 7 of culture, washed with DPBS, and fixed with 4% v/v paraformaldehyde for 20 min at room temperature. Paraformaldehyde was washed with DPBS, and samples were kept at 4 °C overnight. The cells were then permeabilized using 0.2% v/v Triton X-100 for 30 min and washed twice with DPBS. The samples were blocked with 2% v/v BSA for 30 min at room temperature, followed by treatment with 10  $\mu$ g ml<sup>-1</sup> VE-cadherin antibodies for 3 hr at 37 °C. The samples were then washed three times with DPBS and treated with 5  $\mu$ g ml<sup>-1</sup> Donkey anti-Goat IgG (H+L) secondary antibody in DPBS for 45 min at room temperature and washed again three times with DPBS. Finally, the samples were treated with 2  $\mu$ g ml<sup>-1</sup> DAPI solution in DPBS for 10 min at 37 °C and washed with DPBS before microscopy analysis. Fluorescence microscopy was performed on the samples using an inverted fluorescence microscope to observe VE-cadherin (stained in red) at the endothelial cell junctions.

Endothelialization and vascularization assay: To study the endothelization and vascularization of the hydrogels, 200  $\mu$ l of EWMA 7.5% and GelMA 5% pregel solutions were transferred to a 24-well plate and crosslinked. 200  $\mu$ l of as-received Matrigel was also transferred to the well plate, and all samples were sterilized under UV light for 30 min. GelMA and Matrigel are shown to have high compatibility with endothelial cells <sup>[45]</sup>, and both were used as control samples in this experiment. To seed the cells, GFP-HUVECs were suspended in the culture medium, and 100  $\mu$ l of the suspension containing 7.5×10<sup>5</sup> of GFP-HUVECs was transferred to the surface of the samples. The sample plate was then placed on a plate shaker (Thermo Scientific) at 145 rpm and incubated in 5% CO<sub>2</sub> at 37 °C for 1, 2, 3, and 4 days. Cells on the samples were imaged at different incubation times using the fluorescence microscope and ImageJ software was used to estimate the cell spreading area.

Cytocompatibility of the hydrogels in the 3D structure: The cytocompatibility of the EWMA hydrogels was investigated using mouse myoblast cells (C2C12s) encapsulated in the hydrogels (3D culture). C2C12s were obtained from the American Type Culture Collection (ATCC, CRL-2522, Manassas, VA, USA). C2C12s were cultured in a T175 Corning flask using DMEM supplemented with 10% FBS and 1% Pen/Strep in an incubator at 5% CO<sub>2</sub> and 37 °C. At a confluency of 80%, cells were enzymatically detached from the flask using trypsin-EDTA (0.25%) and collected by centrifugation at 1200 rpm for 5 min. GelMA (5% w/v) and EWMA (5, 7.5, and 10% w/v) were dissolved in 100  $\mu$ l of the PI solution (5 mg ml<sup>-1</sup>), and C2C12s at a concentration of 2×10<sup>6</sup> cells ml<sup>-1</sup> were suspended in the pregel solution. The mixtures were gently mixed and loaded into 3 ml syringe and printed using Bio x cell bioprinter. The samples were then crosslinked using a 356 nm UV light at an intensity of 800 mW for 1 min (distance from the light source: 8 cm) and incubated in the incubator at 5% CO<sub>2</sub> and 37 °C to be tested for cell activity.

<u>Cell viability:</u> The well plates were removed from the incubator on day 7 of culture, and the cell-laden hydrogels were washed three times with DPBS.  $0.5~\mu l$  of Calcein and  $2~\mu l$  of Ethidium Homodimer were dissolved in 1 ml of DPBS as a stock solution, and  $500~\mu l$  of

the solution was added to each well. After incubation for 30 min at 37 °C, the dye solution was removed, and the samples were washed three times with DPBS. Finally, fresh DPBS was added to the samples, and live (stained with Calcein-AM in green) and dead (stained with Ethidium Homodimer in red) cells were visualized using an inverted fluorescence microscope (Zeiss Axio Observer 5, Walpole, MA). We employed ImageJ software to enumerate both live and dead cells. Cell viability was subsequently calculated as the ratio of living cells to the total cell count.

Metabolic activity: The metabolic activity of the cell-laden hydrogels was evaluated on days 1, 3, and 7 of culture using the PrestoBlue assay. The PrestoBlue reagent was dissolved in the medium at a ratio of 1:9, and 1 ml of the PrestoBlue solution was added to the samples, followed by incubation at 37 °C for 2 hr. As the cells reacted to the PrestoBlue reagent, the media color changed from violet to pink. Subsequently, 100 μl of media was transferred into the 96-well plates, and the fluorescence intensity resulting from cell activity was measured at excitation/emission wavelengths of 530/590 nm using a microplate reader (Synergy<sup>TM</sup> HTX Multi-Mode Microplate Reader, BioTek Winooski, VT, USA).

DAPI, Phalloidin, and Myosin heavy chain staining: The cell-laden hydrogels were removed from the incubator on day 7 of culture and washed three times with DPBS. Samples were then treated with 4% v/v paraformaldehyde for 20 min at room temperature and washed with DPBS. The samples were permeabilized using 0.2% v/v Triton X-100 for 20 min and washed three times with DPBS. 2% v/v BSA solution was added to the samples and incubated for 1 hr at room temperature. Subsequently, the samples were immersed in a staining solution containing DPBS (1 ml), DAPI (1 μl), Myosin heavy chain (5 μl), and Phalloidin (4 μl) for 30 min at 37 °C and then washed 3 times with DPBS. Actin and nuclei on the samples were stained with Phalloidin and DAPI, respectively, and visualized using an inverted fluorescence microscope.

Evaluation of in vivo biocompatibility and histological analysis: To evaluate biocompatibility and potential toxicity of the EWMA hydrogel, we performed scaffold implantations using two 8 mm incisions in the dorsal region of mice. All animal procedures were conducted under the supervision of the IACUC committee of the Lundquist Institute (#22747). The tested scaffold variations included: 1) control (no injury), 2) 5% GelMA, and 3) 7.5% EWMA. These scaffold samples, shaped as 5 mm diameter and 1 mm height discs, were implanted into dorsal sections of each mouse. Following implantation, the incisions were sutured, and strict adherence to the approved IACUC protocol ensured thorough monitoring of the animals.

After 7 and 30 days of scaffold implantation, mice were euthanized via  $\rm CO_2$  inhalation. The dorsal skin and organs were carefully excised and immediately submerged in a PBS solution. Skin sections containing the scaffolds were dissected, fixed in 10% formalin for a minimum of 48 hours, and subsequently embedded in paraffin. The specimens were then sectioned and subjected to Hematoxylin and Eosin staining or immunofluorescence, following the manufacturer's recommended procedures.

#### Statistical analyses

All results were presented as mean values  $\pm$  standard deviations. GraphPad Prism software was used for the statistical comparison of data. The differences between the data were determined by one-way and two-way ANOVA analyses followed by Tukey's multiple comparison test. Statistical significances were presented as \* (p< 0.05), \*\*\* (p < 0.01), \*\*\*\* (p < 0.001), and \*\*\*\* (p < 0.0001).

# **Supplementary Material**

Refer to Web version on PubMed Central for supplementary material.

# **Acknowledgments**

The authors acknowledge funding from the National Institutes of Health (R01AR073135) and the Terasaki Institute for Biomedical Innovation. MT would like to acknowledge financial support from Fonds de recherche du Québecsanté (FRQS).

# References

- [1]. a) Tavafoghi M, Sheikhi A, Tutar R, Jahangiry J, Baidya A, Haghniaz R, Khademhosseini A, Advanced Healthcare Materials 2020, 9, 1901722;b) Raphael B, Khalil T, Workman VL, Smith A, Brown CP, Streuli C, Saiani A, Domingos M, Materials Letters 2017, 190, 103;c) Yuk H, Zhang T, Lin S, Parada GA, Zhao X, Nature materials 2016, 15, 190; [PubMed: 26552058] d) Briquez PS, Clegg LE, Martino MM, Mac Gabhann F, Hubbell JA, Nature Reviews Materials 2016, 1, 15006;e) Han WM, Heo S-J, Driscoll TP, Delucca JF, McLeod CM, Smith LJ, Duncan RL, Mauck RL, Elliott DM, Nature materials 2016, 15, 477; [PubMed: 26726994] f) Zhao X, Lang Q, Yildirimer L, Lin ZY, Cui W, Annabi N, Ng KW, Dokmeci MR, Ghaemmaghami AM, Khademhosseini A, Advanced healthcare materials 2016, 5, 108; [PubMed: 25880725] g) Wang L, Zhang X, He Y, Wang Y, Zhong W, Mequanint K, Qiu X, Xing M, Advanced Functional Materials 2019, 29, 1806200; h) Liu B, Wang Y, Miao Y, Zhang X, Fan Z, Singh G, Zhang X, Xu K, Li B, Hu Z, Biomaterials 2018, 171, 83; [PubMed: 29684678] i) Chan HF, Zhao R, Parada GA, Meng H, Leong KW, Griffith LG, Zhao X, Proceedings of the National Academy of Sciences 2018, 115, 7503;j) Tavafoghi M, Garg S, Korenevski A, Dittrich M, Colloids Surf B Biointerfaces 2021, 207, 111975; [PubMed: 34371317] k) Tavafoghi M, Darabi MA, Mahmoodi M, Tutar R, Xu C, Mirjafari A, Billi F, Swieszkowski W, Nasrollahi F, Ahadian S, Hosseini V, Khademhosseini A, Ashammakhi N, Biofabrication 2021, 13, 042002.
- [2]. a) Jalili-Firoozinezhad S, Filippi M, Mohabatpour F, Letourneur D, Scherberich A, Materials Today 2020;b) Abeyrathne ED, Lee HY, Ahn DU, Poultry science 2013, 92, 3292.
- [3]. Jalili-Firoozinezhad S, Filippi M, Mohabatpour F, Letourneur D, Scherberich A, Materials Today 2020, 40, 193.
- [4]. Yoon HJ, Shin SR, Cha JM, Lee S-H, Kim J-H, Do JT, Song H, Bae H, PloS one 2016, 11, e0163902.
- [5]. Guo L, Niu X, Chen X, Lu F, Gao J, Chang Q, Biomaterials 2022, 282, 121406. [PubMed: 35182859]
- [6]. Delkash Y, Gouin M, Rimbeault T, Mohabatpour F, Papagerakis P, Maw S, Chen X, Journal of Functional Biomaterials 2021, 12, 45. [PubMed: 34449625]
- [7]. Dong X, Zhang YQ, Journal of Biomedical Materials Research Part B: Applied Biomaterials 2021, 109, 1045. [PubMed: 33252178]
- [8]. a) Chang Q, Darabi MA, Liu Y, He Y, Zhong W, Mequanin K, Li B, Lu F, Xing MMQ, Journal of Materials Chemistry A 2019, 7, 24626;b) Balaji P, Murugadas A, Shanmugaapriya S, Akbarsha MA, Biocatalysis and agricultural biotechnology 2019, 17, 441.
- [9]. Kaipparettu BA, Kuiatse I, Tak-Yee Chan B, Benny Kaipparettu M, Lee AV, Oesterreich S, Biotechniques 2008, 45, 165. [PubMed: 18687065]

[10]. a) Mousseau Y, Mollard S, Qiu H, Richard L, Cazal R, Nizou A, Vedrenne N, Rémi S, Baaj Y, Fourcade L, Funalot B, Sturtz FG, Laboratory Investigation 2014, 94, 340; [PubMed: 24395110] b) Khoo CP, Micklem K, Watt SM, Tissue engineering. Part C, Methods 2011, 17, 895; [PubMed: 21517696] c) Benelli R, Albini A, The International Journal of Biological Markers 1999, 14, 243. [PubMed: 10669953]

- [11]. Gomillion CT, Burg KJL, in Comprehensive Biomaterials II, DOI: 10.1016/ B978-0-08-100691-7.00032-X (Ed: Ducheyne P), Elsevier, Oxford 2017, p. 403.
- [12]. Emamat H, Totmaj AS, Tangestani H, Hekmatdoost A, Clinical nutrition ESPEN 2020, 39, 15. [PubMed: 32859309]
- [13]. Nojima T, Iyoda T, NPG Asia Materials 2018, 10, e460.
- [14]. Jana S, Acta biomaterialia 2019, 99, 53. [PubMed: 31454565]
- [15]. Ren X, Feng Y, Guo J, Wang H, Li Q, Yang J, Hao X, Lv J, Ma N, Li W, Chemical Society Reviews 2015, 44, 5680. [PubMed: 26023741]
- [16]. Rauvala H, Hakomori S Journal of Cell Biology 1981, 88, 149. [PubMed: 7204484]
- [17]. Yue K, Trujillo-de Santiago G, Alvarez MM, Tamayol A, Annabi N, Khademhosseini A, Biomaterials 2015, 73, 254. [PubMed: 26414409]
- [18]. Sewald L, Claaßen C, Götz T, Claaßen MH, Truffault V, Tovar GE, Southan A, Borchers K, Macromolecular bioscience 2018, 18, 1800168.
- [19]. Lien S-M, Ko L-Y, Huang T-J, Acta biomaterialia 2009, 5, 670. [PubMed: 18951858]
- [20]. Peppas NA, Hoffman AS, in Biomaterials science, Elsevier 2020, p. 153.
- [21]. a) Mohaghegh N, Ahari A, Zehtabi F, Buttles C, Davani S, Hoang H, Tseng K, Zamanian B, Khosravi S, Daniali A, Acta Biomaterialia 2023;b) Akbari M, Tamayol A, Laforte V, Annabi N, Najafabadi AH, Khademhosseini A, Juncker D, Advanced functional materials 2014, 24, 4060. [PubMed: 25411576]
- [22]. a) Jiang P, Yan C, Guo Y, Zhang X, Cai M, Jia X, Wang X, Zhou F, Biomaterials science 2019, 7, 1805; [PubMed: 30855616] b) Spicer CD, Polymer Chemistry 2020, 11, 184;c) Peppas NA, Hilt JZ, Khademhosseini A, Langer R, Advanced materials 2006, 18, 1345.
- [23]. Sun J, Wei D, Yang K, Yang Y, Liu X, Fan H, Zhang X, Journal of Materials Chemistry B 2017, 5, 8060. [PubMed: 32264645]
- [24]. a) Brandl F, Sommer F, Goepferich A, Biomaterials 2007, 28, 134; [PubMed: 17011028] b) Nichol JW, Koshy ST, Bae H, Hwang CM, Yamanlar S, Khademhosseini A, Biomaterials 2010, 31, 5536; [PubMed: 20417964] c) Temenoff JS, Steinbis E, Mikos AG, Journal of Biomaterials Science, Polymer Edition 2003, 14, 989. [PubMed: 14661875]
- [25]. Chiu Y-C, Kocagöz S, Larson JC, Brey EM, PLoS One 2013, 8, e60728.
- [26]. a) Massensini AR, Ghuman H, Saldin LT, Medberry CJ, Keane TJ, Nicholls FJ, Velankar SS, Badylak SF, Modo M, Acta biomaterialia 2015, 27, 116; [PubMed: 26318805] b) Pan A, Roy SG, Haldar U, Mahapatra RD, Harper GR, Low WL, De P, Hardy JG, Gels 2019, 5, 43; [PubMed: 31575001] c) Leone G, Consumi M, Aggravi M, Donati A, Lamponi S, Magnani A, Journal of Materials Science: Materials in Medicine 2010, 21, 2491. [PubMed: 20499140]
- [27]. a) Kleinman HK, Martin GR, presented at Seminars in cancer biology 2005;b) Hughes CS, Postovit LM, Lajoie GA, Proteomics 2010, 10, 1886. [PubMed: 20162561]
- [28]. Vestweber D, Arteriosclerosis, thrombosis, and vascular biology 2008, 28, 223. [PubMed: 18162609]
- [29]. Stoker M, Piggott D, Cell 1974, 3, 207. [PubMed: 4611644]
- [30]. a) Kubota Y, Kleinman HK, Martin GR, Lawley TJ, J Cell Biol 1988, 107, 1589; [PubMed: 3049626] b) Mousa SA, Yalcin M, Davis PJ, in Anti-Angiogenesis Strategies in Cancer Therapeutics, DOI: 10.1016/B978-0-12-802576-5.00002-4 (Eds: Mousa SA, Davis PJ), Academic Press, Boston 2017, p. 21.
- [31]. a) LaValley DJ, Reinhart-King CA, Advances in Regenerative Biology 2014, 1, 25247;b) Crosby CO, Zoldan J, Regenerative biomaterials 2019, 6, 61. [PubMed: 30967961]
- [32]. Zhao D, Xue C, Li Q, Liu M, Ma W, Zhou T, Lin Y, Journal of cellular physiology 2018, 233, 3407. [PubMed: 28940499]
- [33]. Breuls RG, Jiya TU, Smit TH, The open orthopaedics journal 2008, 2, 103. [PubMed: 19478934]

[34]. a) Mousseau Y, Mollard S, Qiu H, Richard L, Cazal R, Nizou A, Vedrenne N, Rémi S, Baaj Y, Fourcade L, Laboratory investigation 2014, 94, 340; [PubMed: 24395110] b) Chen X, Yao Y, Liu S, Hu Q, Journal of Biomaterials Applications 2021, 36, 297; [PubMed: 33709831] c) Charbonneau AM, Tran SD, Materials 2020, 13, 4807. [PubMed: 33126509]

- [35]. a) Truong NF, Kurt E, Tahmizyan N, Lesher-Pérez SC, Chen M, Darling NJ, Xi W, Segura T, Acta biomaterialia 2019, 94, 160; [PubMed: 31154058] b) Stowers RS, Allen SC, Suggs LJ, Proceedings of the National Academy of Sciences 2015, 112, 1953;c) Žigon-Branc S, Markovic M, Van Hoorick J, Van Vlierberghe S, Dubruel P, Zerobin E, Baudis S, Ovsianikov A, Tissue Engineering Part A 2019, 25, 1369. [PubMed: 30632465]
- [36]. Montazerian H, Hassani Najafabadi A, Davoodi E, Seyedmahmoud R, Haghniaz R, Baidya A, Gao W, Annabi N, Khademhosseini A, Weiss PS, Advanced Healthcare Materials 2023, 2203404.
- [37]. a) Najafabadi AH, Abadi ZIN, Aikins ME, Foulds KE, Donaldson MM, Yuan W, Okeke EB, Nam J, Xu Y, Weerappuli P, Journal of Controlled Release 2021, 337, 168; [PubMed: 34280415]
  b) Zehtabi F, Montazerian H, Haghniaz R, Tseng K, Mohaghegh N, Mandal K, Zamanian B, Dokmeci MR, Akbari M, Hassani Najafabadi A, Macromolecular Bioscience 2023, 23, 2200333.
- [38]. Popkin BM, Du S, Green WD, Beck MA, Algaith T, Herbst CH, Alsukait RF, Alluhidan M, Alazemi N, Shekar M, Obesity Reviews 2020, 21, e13128. [PubMed: 32845580]
- [39]. Ball H Jr, Winn S, Poultry science 1982, 61, 1041.
- [40]. Tamayol A, Najafabadi AH, Aliakbarian B, Arab-Tehrany E, Akbari M, Annabi N, Juncker D, Khademhosseini A, Advanced healthcare materials 2015, 4, 2146. [PubMed: 26304467]
- [41]. Sun M, Sun X, Wang Z, Guo S, Yu G, Yang H, Polymers 2018, 10, 1290. [PubMed: 30961215]
- [42]. Hoch E, Hirth T, Tovar GEM, Borchers K, Journal of Materials Chemistry B 2013, 1, 5675. [PubMed: 32261191]
- [43]. Rastegar A, Mahmoodi M, Mirjalili M, Nasirizadeh N, Carbohydrate Polymers 2021, 269, 118351. [PubMed: 34294355]
- [44]. Cohen-Kaplan V, Ilan N, Vlodavsky I, Frontiers in Oncology 2020, 10, 2. [PubMed: 32038981]
- [45]. a) Khayat A, Monteiro N, Smith E, Pagni S, Zhang W, Khademhosseini A, Yelick P, Journal of dental research 2017, 96, 192; [PubMed: 28106508] b) Ponce ML, in Angiogenesis Protocols, Springer 2009, p. 183.

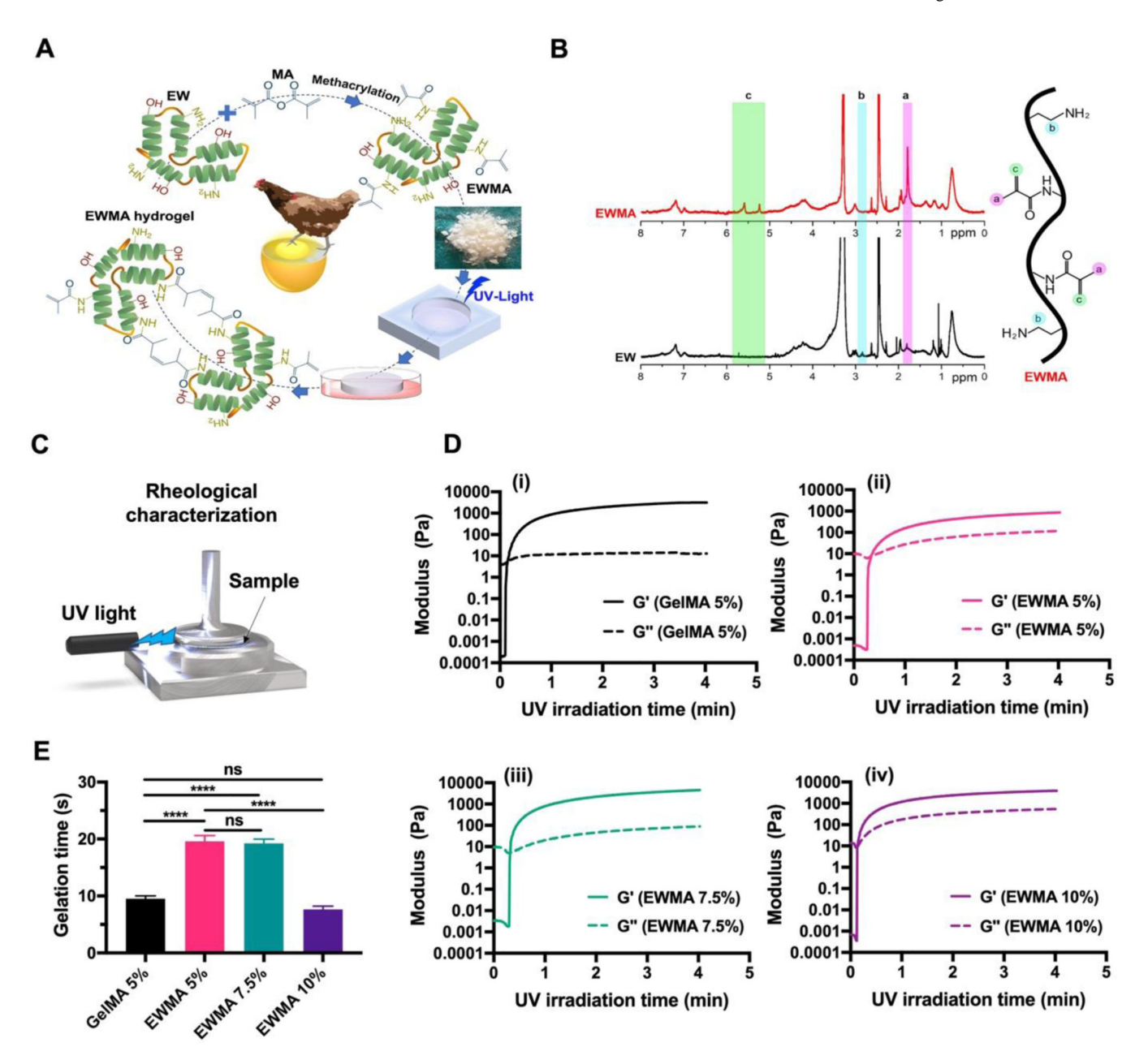


**Figure 1. Synthesis, chemical characterization, and gelation kinetics of EWMA.**(A) Schematic illustrating the methacryloyl modification and crosslinking of EW with UV light to form EWMA hydrogels. (B) <sup>1</sup>H-NMR spectra of pristine and methacryloyl-modified EW with a substitution degree of 74.6%. Solutions were prepared in D<sub>2</sub>O, and the measurements were performed at 4 °C. Peaks corresponding to methacrylate groups were shown in green (5–6 ppm) and pink (1.7–1.9 ppm). Amino groups were shown in blue (2.7–3 ppm). (C-E) Rheological characterization of hydrogel crosslinking kinetics, including GelMA 5% w/v and EWMA 5, 7.5, and 10% w/v. (C) Schematic illustration of the experimental setup. (D) Real-time monitoring of crosslinking kinetics and the variation of storage and loss modulus with UV irradiation time. i) GelMA 5%, ii) EWMA 5%, iii) EWMA 7.5%, and iv) EWMA 10%. (E) Comparing the gelation time of 5% GelMA with

varying concentrations of EWMA hydrogels. Asterisks show the results that are statistically significantly different with p-values less than 0.001~(\*\*\*), and ns shows the non-significant differences.

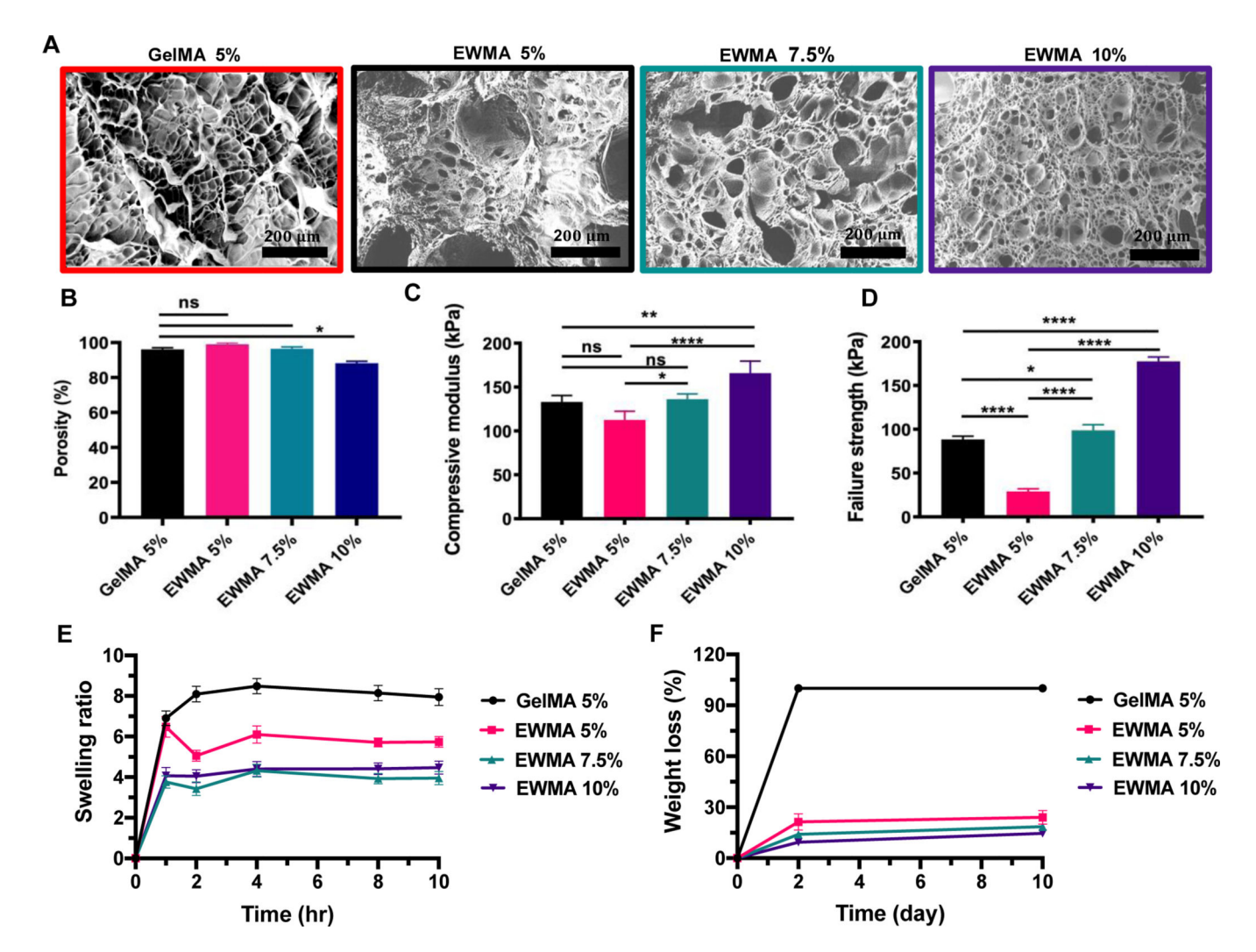


Figure 2. Mechanical, physical, and morphological characterization of the EWMA hydrogels at different concentrations (5%, 7.5%, and 10% w/v) and GelMA hydrogel at 5% w/v. (A) Representative SEM images of hydrogels. (B) The porosity of the hydrogels was determined by analyzing SEM images with ImageJ software. (C, D) Compressive modulus and failure strength for hydrogels after 2 hr incubation in DPBS. (E) The time-dependent swelling ratio of the hydrogels. (F) Time-dependent degradation of UV crosslinked hydrogels in DPBS with collagenase II (2.5 U/ml) at 37 °C. Mean values from a minimum of four replicates  $\pm$  standard deviations are presented. Asterisks (\*) indicate statistically significant differences (p < 0.05), while 'ns' denotes non-significant differences. 0.01 (\*\*), and 0.0001(\*\*\*\*).

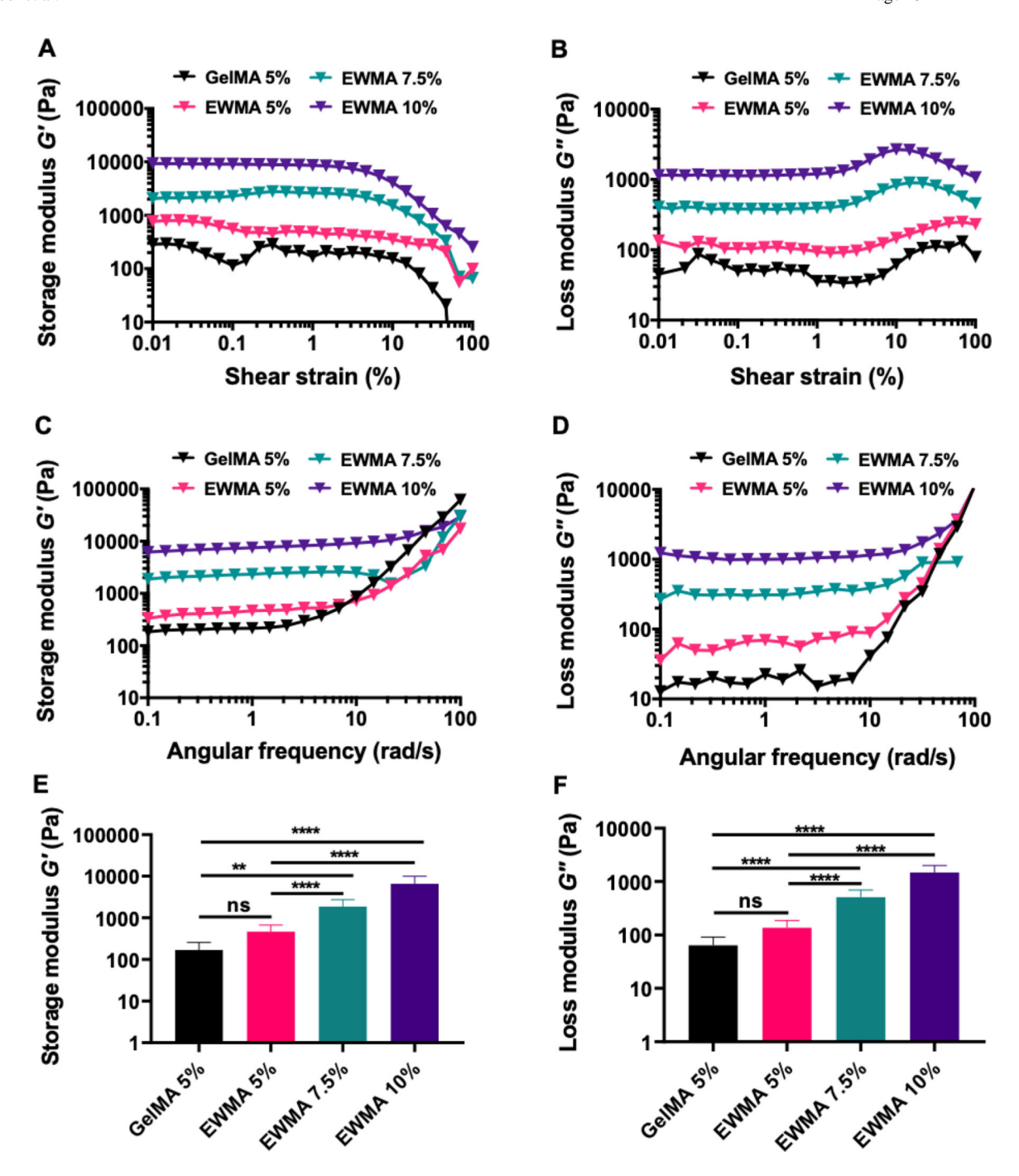


Figure 3. Rheological characterization of crosslinked EWMA hydrogels at different concentrations (5%, 7.5%, and 10% w/v) and GelMA hydrogel at 5% w/v.

(A, B) Storage and loss modulus of the hydrogels *versus* shear strain. (C, D) Storage and loss modulus of the hydrogels *versus* angular frequency. (E, F) Storage and loss modulus of the hydrogels at strain=0.1% and angular frequency=1 rad/s. Data represent the mean values of a minimum of five replicates  $\pm$  standard deviations. Statistically significant differences are denoted by asterisks (\*\* p < 0.01 and \*\*\*\* p < 0.0001), while 'ns' indicates non-significant differences.

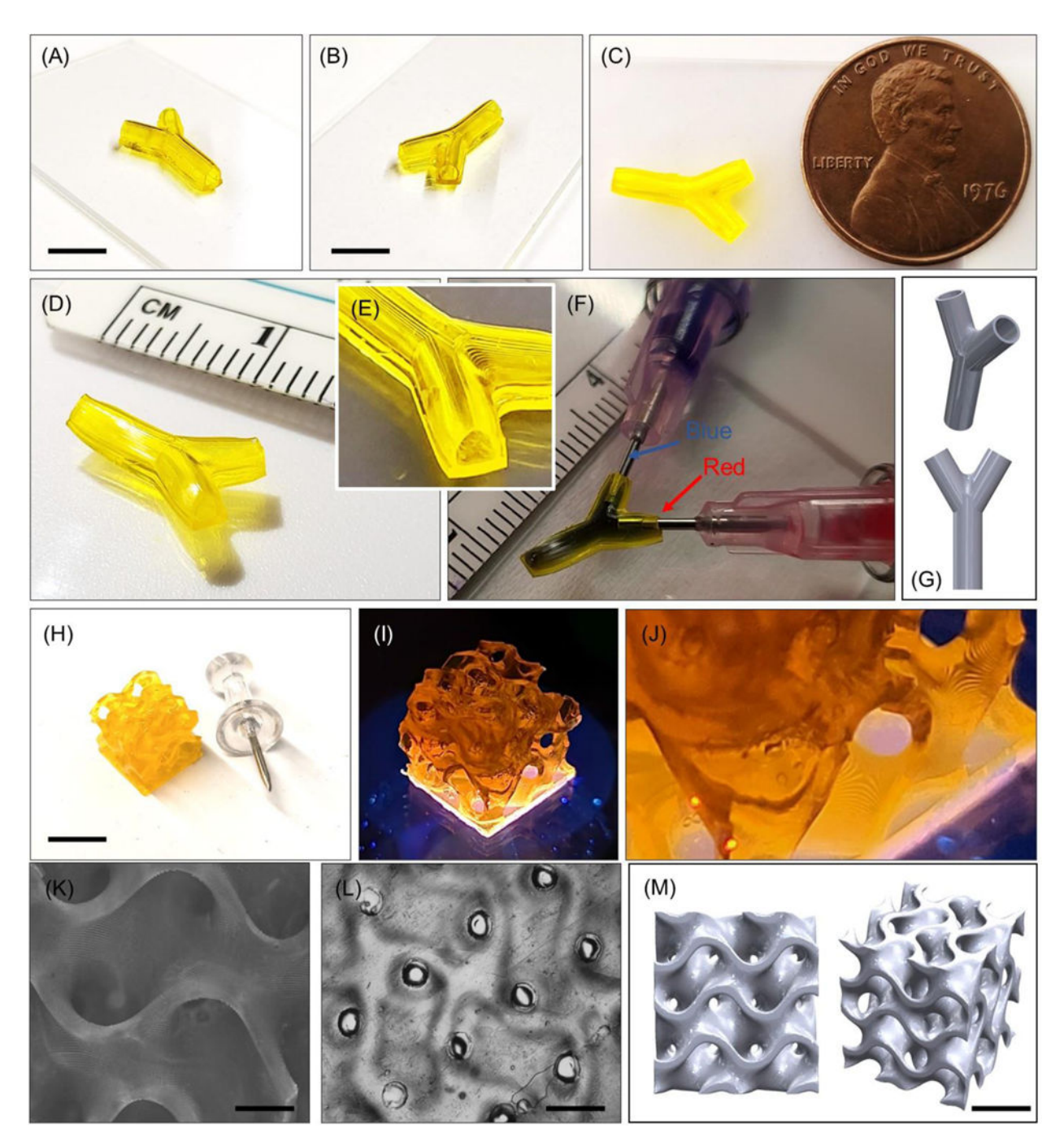


Figure 4. Light-based additive manufacturing of EWMA constructs using DLP SLA; (A), (B), and (C) various isometric and top views of the printed Y-shaped perfusable hydrogel construct, scale bar 4 mm; (D) close-up view of the bifurcation; (E) close-up visualization of the printed layers and the staircase effect observed in the channel walls; (F) red and blue dye perfusion in the bifurcation and demonstration of construct perfusability; (G) 3D design of the Y-shaped bifurcation; (H) A printed gyroid structure, showcasing 8 unit cells across with a 500  $\mu$ m wall thickness, illustrates the capability of printing intricate structures using EWMA with different printing method (Scale bar: 4 mm); (I) zoomed-in

structure of gyroid print with 8-unit cells; (**J**) optical microscopy image of gyroid structure showing one unit cell of gyroid 3D structure printed and the layering artifacts from the DLP printer; (**K**) visualizing strut distance in EWMA-printed structure; (**L**) strut distance and pore structure in EWMA-printed scaffold; and (**M**) representation of the 3D structure printed by DLP printer using EWMA as bioink. Scale bar 4 mm.

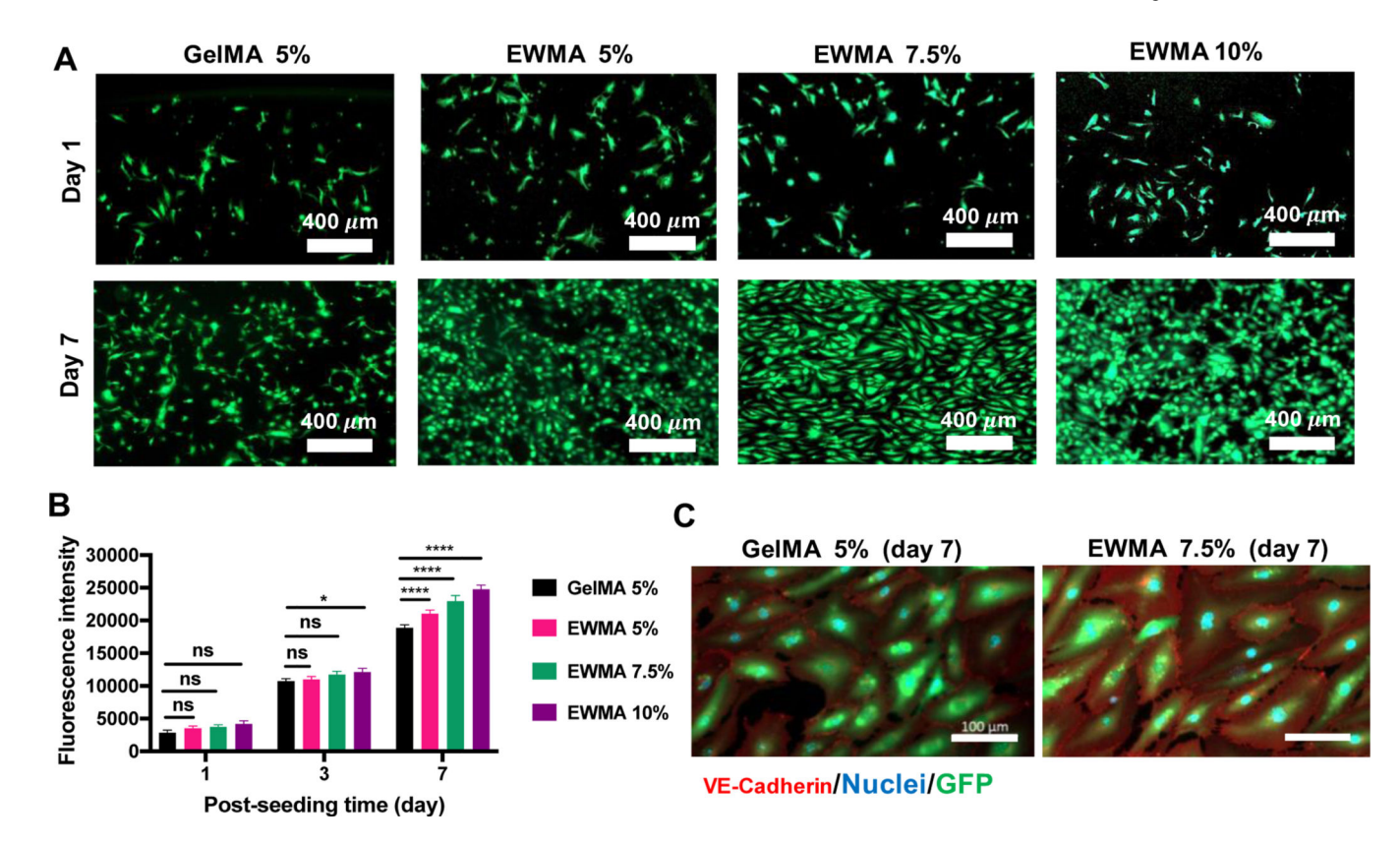


Figure 5. The cytocompatibility of EWMA hydrogels at different concentrations (5%, 7.5%, and 10% w/v) and GelMA hydrogel at 5% w/v with GFP-HUVECs in a 2D culture.

(A) Fluorescence images of hydrogels seeded with GFP-HUVECs on days 1 and 7 of culture. (B) Metabolic activity of GFP-HUVECs seeded on the surface of the hydrogels on days 1, 3, and 7 of culture. (C) Fluorescence images of intact and VE-cadherin/DAPI-stained GFP-HUVECs seeded on EWMA 7.5% and GelMA 5% (control) on day 7 of culture, showing HUVECs remained functional on the surface of EWMA and expressed VE-cadherin to form adherents' junctions between the endothelial cells (red: VE-cadherin, blue: nuclei and green: GFP).

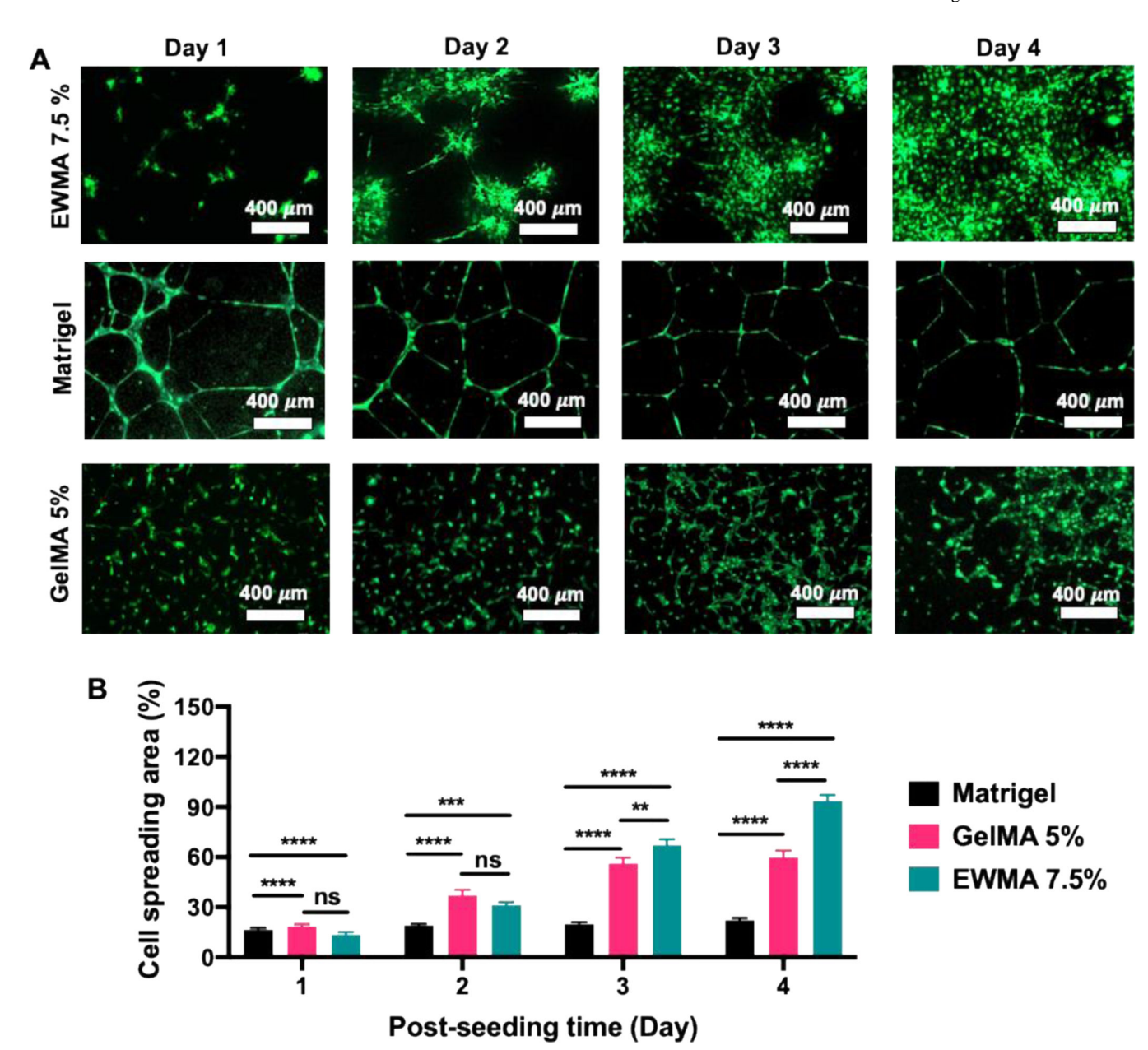


Figure 6. The endothelialization and vascularization of EWMA 7.5% w/v, GelMA 5% w/v, and Matrigel hydrogels using GFP-HUVECs seeded on the surface of the hydrogels. (A) Fluorescence images of the hydrogels seeded with GFP-HUVECs on days 1, 2, 3, and 4 of culture. (B) Cell spreading area on the hydrogel surface at different incubation times. Higher cell spreading on EWMA compared to GelMA and Matrigel shows higher vascularization of the EWMA hydrogel. The EWMA and GelMA hydrogels were crosslinked with UV light at an intensity of 800 mW for 1 min. Matrigel was used in its as-received form. All samples were seeded with  $7.5\times10^5$  GFP-HUVECs and placed on a plate shaker in the incubator at 145 rpm and 37 °C. The data represent mean values from a minimum of four replicates  $\pm$  their respective standard deviations. Asterisks (\*) indicate statistically significant differences, with p-values denoted as follows: \*p < 0.01, \*\*\* p < 0.001, \*\*\* p < 0.001, \*\*\* p < 0.001; 'ns' indicates non-significant differences.

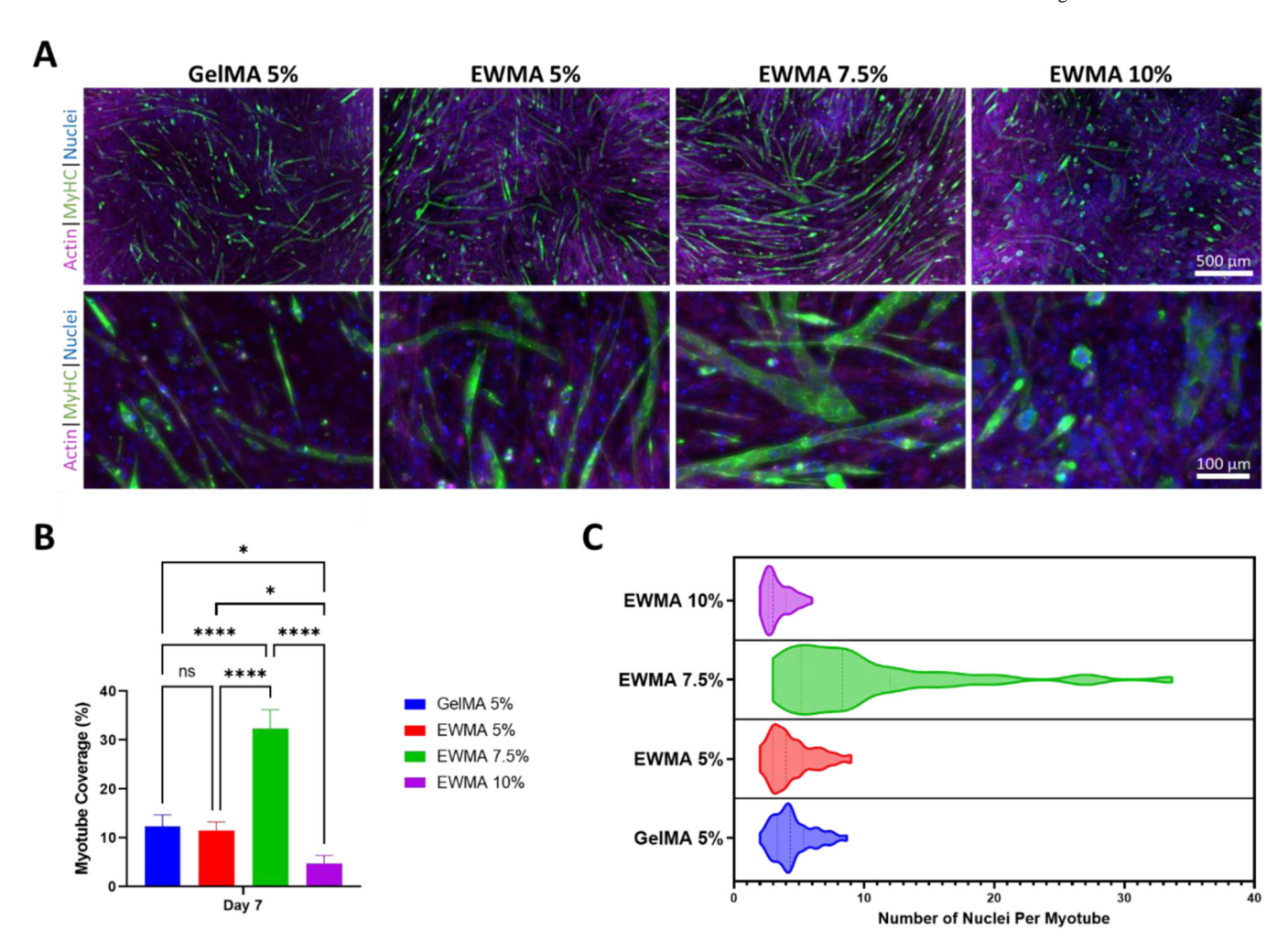


Figure 7. The cytocompatibility of EWMA hydrogels at different concentrations (5%, 7.5%, and 10% w/v) and GelMA hydrogel at 5% w/v with C2C12 cells in a 3D culture.

(A) Immunofluorescent stained images of C2C12-laden hydrogels on day 7 of post-differentiation induction. Myosin heavy chain (MyHC) is stained in green; actin is stained with Phalloidin in magenta, and nuclei are stained with DAPI in blue. (B) Total myotube coverage percentages of differentiated C2C12 cells on day 7 post differentiation induction. (C) Average nuclear distribution in differentiated C2C12 cell-derived myotubes. The data represent mean values from a minimum of four replicates ± their respective standard deviations. Asterisks show results that are statistically significantly different with p-values less than 0.01 (\*\*\*), 0.001 (\*\*\*\*), and 0.0001(\*\*\*\*\*), and ns show non-significant differences.

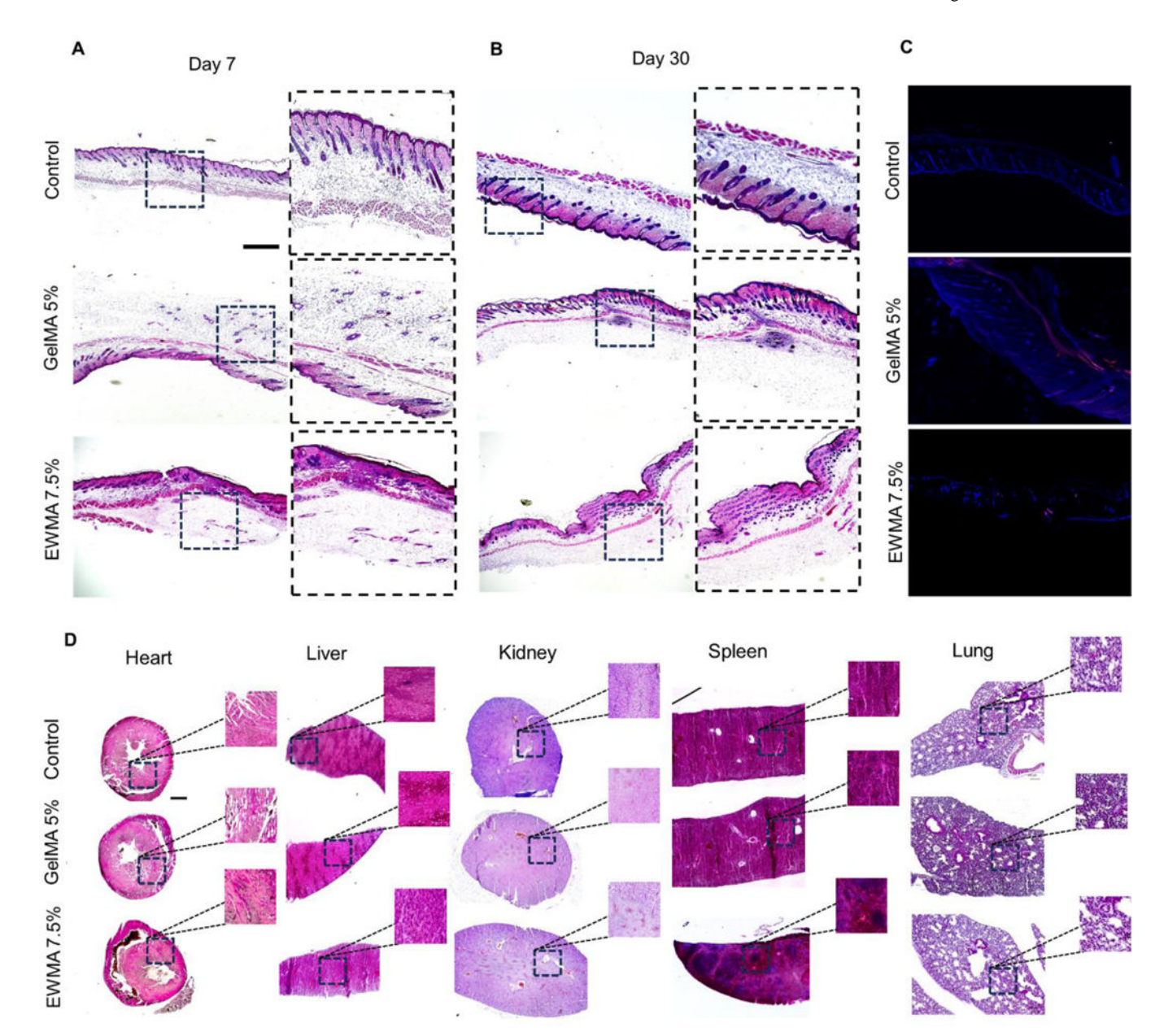


Figure 8. Biocompatibility study of EWMA 7.5% using mouse subcutaneous implant in vivo. Cross-sectional histological images of H&E stained skin on (A) day 7 and (B) day 30 after initial implantation. (scale bar:  $200 \, \mu m$ ). (C) Immunohistochemical staining was conducted on the subcutaneous implants using F4/80 and CD80 markers, accompanied by nuclear staining. Widefield fluorescent images were captured seven days after subcutaneous implantation, with color-coding as follows: Red corresponds to F4/80-macrophages, green to CD80, and blue to DAPI. (Scale bar:  $200 \, \mu m$ ). (D) H&E staining of heart, kidney, spleen, liver, and lung for the toxicity effect study (scale bar:  $200 \, \mu m$ ).